SCIENTIFIC OASIS

Spectrum of Mechanical Engineering and Operational Research

Journal homepage: www.smeor-journal.org
eISSN: 3042-0288

Mechanical Analysis of Sandwich Plates with Lattice Metal Composite Cores

Federico Marino[1], Marzena Pawlik[1], Stefano Valvano[1,*]

[1] College of Science and Engineering, University of Derby, Markeaton Street, Derby, DE22 3AW, UK

ARTICLE INFO

Article history:
Received 21 February 2024
Received in revised form 19 April 2024
Accepted 19 May 2024
Available online 22 May 2024

Keywords:
BCC; Lattice; Homogenised; Multiscale; Sandwich Structure; Finite Element Analysis.

ABSTRACT

This study investigates the modal and static behaviour of sandwich panels with lattice core structures, comparing the real cellular solid structures' response with an equivalent homogenised model. The mechanical model has been described through the Finite Element Method (FEM), and 3D elements with reduced integration have been employed to guarantee an accurate description of skins and the lattice geometry. Different Body Centred Cubic (BCC) cell configurations have been considered: standard metal BCC cell, metal BCC cell with waved struts, standard metal composite BCC cell. Depending on the configuration, the homogenised materials showed isotropic or orthotropic properties. The composite core has been modelled using two different materials, namely an Aluminium matrix with an AlSiC filler, which is enclosed inside the other hence constituting the BCC cell's strut. A free-vibration and static analysis parametric study has been conducted varying the strut's diameter, the strut's waviness and the thickness ratio of the composite struts. For the static analysis, a multiscale approach has been adopted; a first step considering the whole homogenised sandwich panel and a second step comparing the multiscale results of the homogenised model and those of real structure considering a small portion of the panel. Results reveal insights into the effects of core structure parameters on the mechanical response of sandwich panels, aiding in design optimisation and structural enhancement.

1. Introduction

In recent years, the increasing demand for lowering the carbon footprint of the major transportation systems is causing their respective industries to search for novel alternative materials and approaches [1]. The development of Additive Manufacturing (AM) technologies has brought large interest in 3D printed structures, resulting in lightweight and high-performing structures. According to the ISO/ASTM 52900:2021 standard, the AM process is defined as: "the process of joining materials to make parts from 3D model data, usually layer upon layer, as opposed to subtractive manufacturing and formative manufacturing methodologies" [2]. These technologies allow the designing and manufacturing of complicated geometries, otherwise unfeasible with the use

* *Corresponding author.*
E-mail address: s.valvano@derby.ac.uk

https://doi.org/10.31181/smeor1120244

of standard techniques, contributing also to material reduction via topological optimisation procedures [3–5]. For that reason, a wide range of industries makes use of AM for a large number of applications, such as: aerospace, automotive, biotechnology and building among others [6–9]. The intrinsic process of printing structures layer by layer enables the design of lattice structures. These structures belong to the family of cellular solids [10], together with foams and meshes [11–14]. The basic idea behind the concept of lattice structures is the design of a reticular frame made of unit cells which are periodically arranged in the three-dimensional space. Given the freedom of design that the AM offers, several unit cells have been created by arranging the cell's struts in different ways, such as: BCC, Face Centred Cubic (FCC) and octahedron, to name a few [15–18]. Moreover, focusing on a specific cell design, the properties of the single cell may be changed by introducing geometrical or material-depending parameters. For example, in the BCC cell case, the original structure can be modified by introducing waved struts, thus obtaining a waved BCC cell [19], or by introducing multilayered struts with different materials, thus obtaining a composite BCC cell [20]. It is then clear that this design freedom allows one to tailor the mechanical and thermal properties of a specific component in its working environment, for example with respect to standard metallic materials, composite laminates or honeycombs [21–24].

Despite the convenience of dealing with a great number of cell types, hence being capable of designing very complicated structures, lattice materials present a major drawback when recurring to simulations. In fact, the mechanical analysis of actual structures made up of a great number of cells is computationally expensive and often non-feasible, thus the developing of novel approaches is currently being studied [25]. One of the established methods is the well-known Representative Volume Element (RVE). According to Hill [26], the RVE is defined as the smallest volume element that is sufficiently large to be statistically representative of the entire domain. This is due to the need to effectively represent the behaviour of the structure, taking into account the micromechanics involved, e.g. voids and defects [27]. This can be achieved by making use of the correct choice of the dimension of the RVE [28,29] and the implementation of periodic boundary conditions [30]. Despite its convenience, it must be said that this kind of approach is not representative if complex cellular topologies are implemented. An equivalent approach can be found in the homogenisation techniques, where a single volume element is periodically repeated. Several works are available regarding the homogenisation, such as Ptochos et al. [31], Valvano [20], Arabnejad et al. [32] and Craster et al. [33]. Moreover, a simplified model for BCC lattice cells and porous materials has been used in the work of Alaimo et al. [34], Mantegna et al. [35] and Tumino et al. [19].

Among lightweight structures, sandwich panels have shown to be a competitive alternative already [36] and a large number of solutions have been studied for sandwich core characterisation [37]. In this study, a parametric analysis was performed on the modal and static responses of sandwich panels with lattice core structures, comparing them to a homogenized model. A FEM approach with 3D quadratic elements and reduced integration was employed for accuracy. The core consisted of BCC cells with three strut designs: straight aluminium struts, composite layered struts, and waved aluminium struts. The studied parameters included strut diameter, waviness, and thickness ratio. Apart from the modal analysis, the static analysis has used a multiscale approach, where a full homogenised panel has been modelled first, and then the corresponding local zones have been modelled for both the homogenised and real sandwich plates.

2. Mechanical problems for sandwich plates

In the present work new results of sandwich plates embedding lattice composite metal cells are presented, in particular the attention is focused on the static analysis and the free-vibration analysis, the corresponding governing equations can be derived from the Principle of Virtual Displacement (PVD) as follows, see for examples [38,39]:

$$\delta L_{int} + \delta L_{in} = \delta L_{ext} \quad (1)$$

Where δ is the virtual variation, L_{int} the internal work, L_{in} the inertial work and L_{ext} the external forces work. If the inertial work is neglected, it possible to write the PVD definition for static analysis:

$$\int_V \delta\boldsymbol{\epsilon}^T \boldsymbol{\sigma}\, dV = \int_\Omega \delta\boldsymbol{u}^T p\, d\Omega \quad (2)$$

Where $\boldsymbol{\sigma}$ and $\boldsymbol{\epsilon}$ are the stress and strain vectors, T stands for transpose, V is volume structural domain. Considering a distributed pressure as external force contribution, p is the applied pressure, Ω is the surface domain and $\boldsymbol{u}=(u,v,w)$ is the three-dimensional mechanical displacement vector. The governing equation of the static analysis can be expressed in compact form as follows:

$$\delta\boldsymbol{U}: \boldsymbol{K}\,\boldsymbol{U} = \boldsymbol{P} \quad (3)$$

Where $\boldsymbol{K}$ and $\boldsymbol{P}$ are the stiffness matrix and the load vector respectively; $\boldsymbol{U}=(U,V,W)$ are the displacement unknowns.

In Eq. 1, if the external load contribution is neglected, it is possible to obtain the PVD definition for free-vibration analysis as follows:

$$\int_V \delta\boldsymbol{\epsilon}^T \boldsymbol{\sigma}\, dV - \omega^2 \int_V \rho\, \delta\boldsymbol{u}^T \boldsymbol{u}\, dV = 0 \quad (4)$$

Where ρ is the material density and ω is the circular frequency. The governing equation of the free-vibration analysis can be expressed in compact form as follows:

$$\delta\boldsymbol{U}: (\boldsymbol{K} - \boldsymbol{\lambda}\,\boldsymbol{M})\,\boldsymbol{U} = 0 \quad (5)$$

Where $\boldsymbol{M}$ is the mass matrix, $\boldsymbol{\lambda}$ are the eigenvalues and the mechanical unknowns $\boldsymbol{U}$ are the eigenvectors of the system. The definition of the natural frequencies $\boldsymbol{f}$ can be obtained from the eigenvalues as follows:

$$\boldsymbol{\omega}_n = \sqrt{\boldsymbol{\lambda}} \quad ; \quad \boldsymbol{f} = \frac{\boldsymbol{\omega}_n}{2\pi} \quad (6)$$

Where $\boldsymbol{\omega}_n$ are the circular natural pulsations.

In this work the mechanical displacements $\boldsymbol{u}=(u,v,w)$ are expressed through a 3D approach; the Finite Element Method (FEM) is employed to the describe the mechanical displacements brick and tetrahedral second order elements have been used:

$$\boldsymbol{u}^d[x(\xi,\eta,\zeta), y(\xi,\eta,\zeta), z(\xi,\eta,\zeta)] = \boldsymbol{U}^d \sum_{d=1}^{n} \boldsymbol{N}^d(\xi,\eta,\zeta) \quad (7)$$

Where the $\boldsymbol{N}^d$ are the classical Lagrangian shape functions defined in the local finite element reference system (ξ, η, ζ). In the literature it is well known that the finite element accuracy can be affected by the shear and membrane locking numerical phenomena. To overcome this issue the authors adopted the reduced integration method [40].

In this work the geometrical linear relations have been considered for the evaluation of the mechanical strains $\boldsymbol{\epsilon}$; the strains are related to the mechanical displacements $\boldsymbol{u}$ as follows:

$$\begin{bmatrix} \epsilon_{xx} \\ \epsilon_{yy} \\ \epsilon_{xy} \\ \epsilon_{xz} \\ \epsilon_{yz} \\ \epsilon_{zz} \end{bmatrix} = \begin{bmatrix} \frac{\partial u}{\partial x} \\ \frac{\partial v}{\partial y} \\ \frac{\partial u}{\partial y} + \frac{\partial v}{\partial x} \\ \frac{\partial u}{\partial z} + \frac{\partial w}{\partial x} \\ \frac{\partial v}{\partial z} + \frac{\partial w}{\partial y} \\ \frac{\partial w}{\partial z} \end{bmatrix} \quad (8)$$

The mechanical stresses are described by the Hooke's law as $\boldsymbol{\sigma}^k = \boldsymbol{C}^k \boldsymbol{\epsilon}^k$, where *k* stands for the lamina number along the sandwich plate stacking sequence. Some of the considered equivalent lattice structure materials need an orthotropic material properties description [20] as follows:

$$\boldsymbol{C}^k = \begin{bmatrix} C_{11} & C_{12} & C_{16} & 0 & 0 & C_{13} \\ C_{12} & C_{22} & C_{26} & 0 & 0 & C_{23} \\ C_{16} & C_{26} & C_{66} & 0 & 0 & C_{36} \\ 0 & 0 & 0 & C_{55} & C_{45} & 0 \\ 0 & 0 & 0 & C_{45} & C_{44} & 0 \\ C_{13} & C_{23} & C_{36} & 0 & 0 & C_{33} \end{bmatrix}^k \tag{9}$$

3. Free-vibration Analysis

A free vibration analysis campaign has been conducted to evaluate the natural frequencies and the vibrating modes of a rectangular sandwich panel. In this campaign, the first ten frequencies are evaluated. The sandwich panel's geometrical dimensions are: a=1 m, b=0.6 m, h_{skin}=0.001 m, h_{core}=0.008 m. While the mechanical properties of top and bottom skins are: E_1=50 GPa, E_2=E_3=10 GPa, G_{12}=50 GPa, G_{13}=G_{23}=10 GPa, ν_{12}= ν_{13}= ν_{23}=0.25, ρ=1700 kg/m^3. Regarding the specific mechanical properties of the core and the cells, those have been adopted from the previous work of Valvano [20]. For the first campaign, the strut's diameter has been varied, in order to capture the frequency dependence. The chosen diameters are: D_1=1 mm, D_2=1.5 mm, D_3=2 mm.

3.1 Isotropic Core

A convergence analysis has been conducted in order to evaluate the mesh setup that best fits the problem. Implemented meshes are made of 8, 10, 12 and 16 brick elements along the sides of the panel, while four elements have been used for each layer. A simply supported boundary condition has been imposed along the lateral sides of the panel. In Table 1 the convergence analysis is represented in tabular form for D=1 mm. While in Figure 1 an example of the implemented lattice cell is shown. The core is made of stainless-steel material and after homogenisation behaves isotropically. The homogenised properties of the BCC lattice cell have been evaluated in the previous work of Valvano [20] and adopted here (see Table 2).

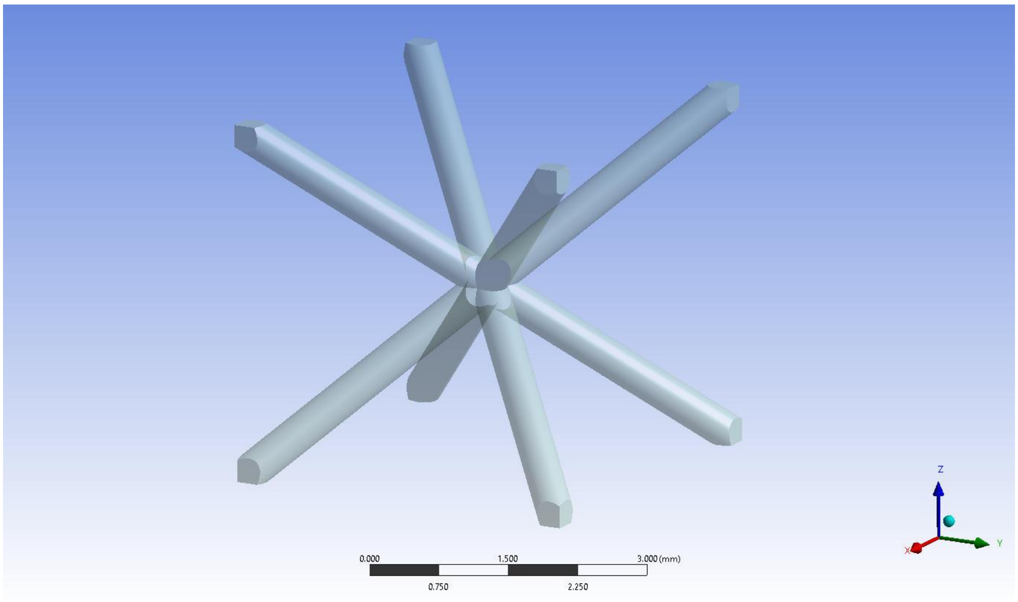

Fig. 1. Example of BCC lattice cell with straight struts, D=1 mm

Table 1
Sandwich plate with lattice core. Convergence analysis in respect to the 16x16 mesh, D=1 mm

Mode	1	2	3	4	5	6	7	8	9	10
8x8	57.47	137.39	159.4	229.35	275.34	332.92	359.51	396.92	470.72	519.32
err %	0.0043	0.0633	0.0632	0.1345	0.335	0.331	0.5548	0.4523	1.0312	1.3524
10x10	57.46	137.33	159.34	229.11	274.75	332.23	358	395.62	467.69	513.73
err %	0.0013	0.0213	0.0226	0.0317	0.1199	0.1228	0.1319	0.124	0.3804	0.2603
12x12	57.46	137.31	159.32	229.06	274.55	331.99	357.68	395.3	466.61	512.75
err %	0.0005	0.008	0.0087	0.0099	0.0462	0.048	0.0416	0.0427	0.1488	0.07

Table 2
Homogenised properties of the BCC cell with straight struts for different diameters

D [mm]	1	1.5	2
ρ [kg/m^3]	386.82	828.41	1396.99
E [MPa]	70.764	408.59	1473.7
ν	0.492	0.479	0.46
G [MPa]	1263.8	2927.7	5384.3

A 12x12 mesh guarantees the convergence of the solution for all the considered natural frequencies. Table 3 presents the corresponding natural frequencies in relation to the diameter variation. The sandwich panes with the smallest diameter (1 mm) shows the highest natural frequencies for all modes tested. This is due to the lowest the density and mechanical properties across the three BCC cells simulated. Figure 2 shows examples of the vibrating modes for 2nd mode, 1.5 mm strut (a), 6th mode, 1 mm strut (b).

Table 3
Sandwich plate with lattice cell. Natural frequencies f [Hz] for different strut diameters in mm

Mode	1	2	3	4	5	6	7	8	9	10
D=1	57.46	137.31	159.32	229.06	274.55	331.99	357.68	395.3	466.61	512.75
D=1.5	48.86	114.83	133.68	195.07	226.86	276.46	303.09	334.86	384.05	437.86
D=2	44.47	101.73	120.85	177.65	197.28	248.18	272.74	304.6	331.14	399.19

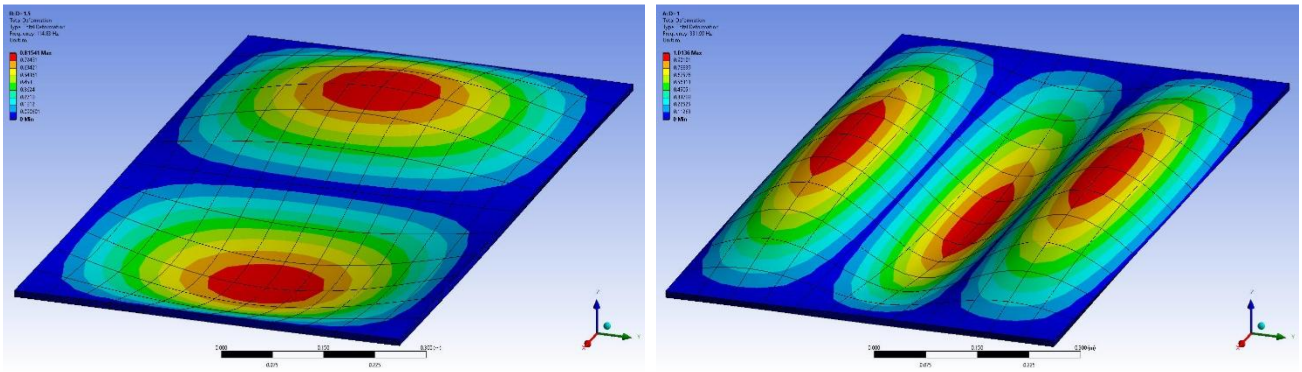

(a) (b)

Fig. 2. Sandwich plate with lattice cell. (a) 2nd vibrating mode for D=1.5 mm, (b) 6th vibrating mode for D=1 mm

3.2 Composite Core

This subsection focuses on understanding the dependence of the natural frequencies on the lattice cell's composite materials composed of a core surrounded by an outer layer. In order to do so, a sandwich panel with a composite lattice structure core has been analysed. In Figure 3 the composite BCC lattice cell is shown. The cell's outer layer is made up of an isotropic aluminium, while the inner layer is made up of an assumed isotropic metal matrix composite AlSiC. The mechanical properties of both materials were taken by the work of Valvano [20]. The properties of the homogenised core were obtained to simulate a cell with layered struts in the radial direction. The analysis setup is the same stated above, two diameters have been studied: D=1 mm and D=2 mm. Lastly, three configurations of layered struts have been analysed, with a thickness ratio of: $\bar{t} = 0.25$, $\bar{t} = 0.50$, $\bar{t} = 0.75$, where $\bar{t}$ is defined as $\bar{t} = D_{comp}/D_{tot}$ and the volume fraction V_f of the AlSiC has been varied as well, that is: V_f=0.41, V_f=0.54, V_f=0.70. In Table 4 and Table 5 the natural frequencies of the analysed cases are presented, while in Figure 4 and Figure 5, two examples of the vibrating modes are presented for both diameters.

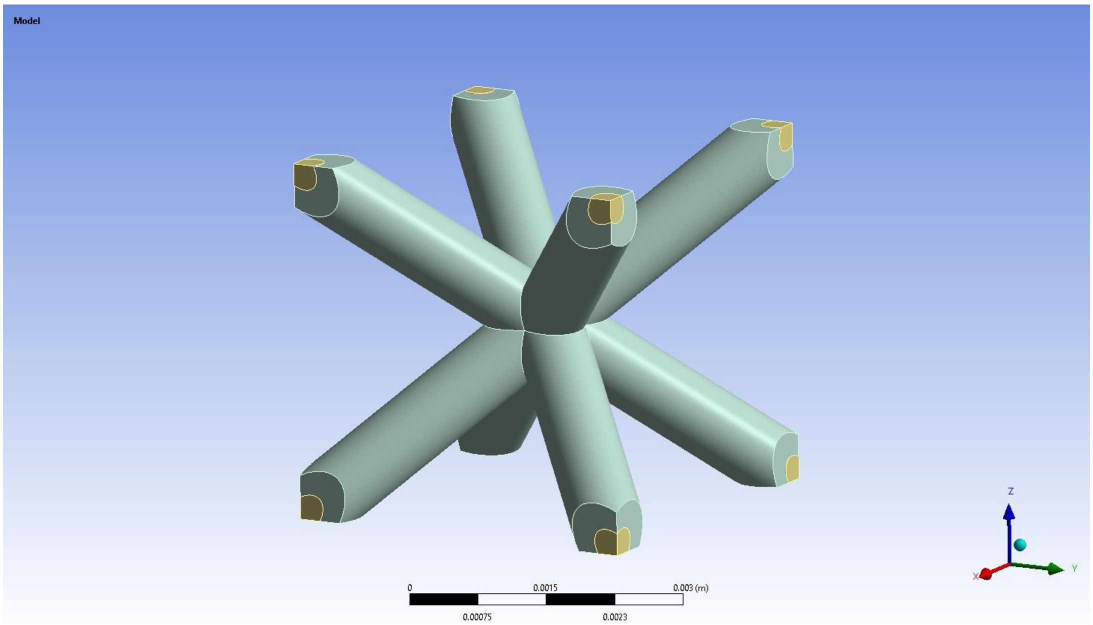

Fig. 3. Representation of the composite BCC lattice cell

Table 4
Natural frequencies of the panel in Hz, in respect to the diameter ratio and the volume fraction for D=1 mm

Mode		1	2	3	4	5	6	7	8	9	10
	V_f=41%	67.85	162.75	189.55	269.35	325.75	395.73	419.37	465.87	551.17	598.93
t=0.25	V_f =54%	67.87	162.82	189.6	269.52	325.93	395.84	419.73	466.16	551.68	599.52
	V_f =70%	67.89	162.87	189.62	269.65	326.07	395.92	420.02	466.39	552.08	600
	V_f =41%	67.88	162.82	189.5	269.69	326.05	395.68	420.28	466.46	552.41	600.53
t=0.5	V_f =54%	67.97	163.02	189.63	270.24	326.54	395.94	421.39	467.34	553.73	602.37
	V_f =70%	68.04	163.17	189.71	270.66	326.86	396.07	422.23	468	554.61	603.77
	V_f =41%	67.91	162.85	189.38	270.12	326.23	395.41	421.34	467.1	553.47	602.47
t=0.75	V_f =54%	68.11	163.22	189.62	271.17	326.91	395.74	423.28	468.67	555.19	605.71
	V_f =70%	68.28	163.46	189.76	271.96	327.25	395.82	424.66	469.76	556.04	608.06

Table 5
Natural frequencies of the panel in Hz, in respect to the diameter ratio and the volume fraction for D=2 mm

Mode		1	2	3	4	5	6	7	8	9	10
	V_f=41%	57.06	134.46	157.98	227.72	266.88	328.45	353.49	393.34	452.7	510.71
t=0.25	V_f =54%	57.16	134.6	158.12	228.11	267.01	328.62	354.04	393.88	452.83	511.64
	V_f =70%	57.24	134.7	158.23	228.43	267.1	328.72	354.48	394.3	452.89	512.39
	V_f =41%	57.34	134.73	158.29	228.89	266.78	328.57	355.01	394.84	452.1	513.52
t=0.5	V_f =54%	57.72	135.27	158.88	230.41	267.27	329.29	357.13	396.96	452.52	517.1
	V_f =70%	58.02	135.7	159.33	231.67	267.61	329.78	358.87	398.67	452.72	520.03
	V_f =41%	57.83	135.22	158.99	230.89	266.71	329.24	357.55	397.6	451.25	518.26
t=0.75	V_f =54%	58.7	136.48	160.54	234.42	267.89	331.4	362.36	402.73	452.24	526.42
	V_f=70%	59.43	137.51	161.78	237.35	268.75	333.04	366.32	406.92	452.76	533.14

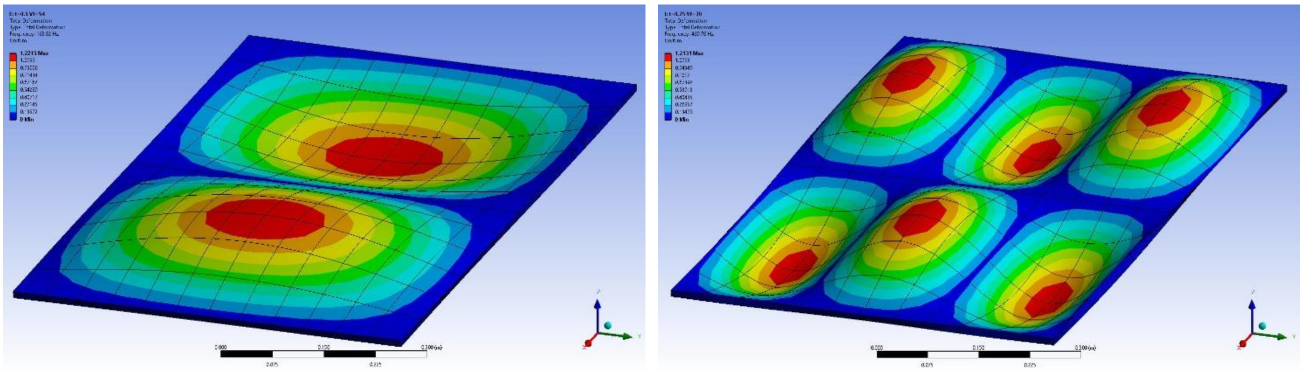

(a) (b)

Fig. 4. Sandwich plate with lattice cell. (a) 2nd vibrating mode with $\bar{t}$=0.5, Vf=54%, (b) 8th vibrating mode with $\bar{t}$=0.75, Vf =70%. D=1 mm

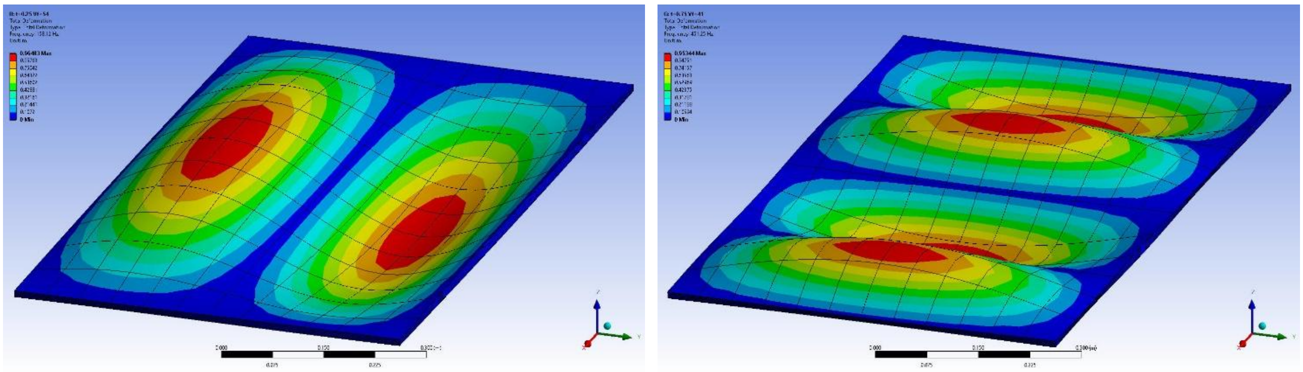

(a) (b)

Fig. 5. Sandwich plate with lattice cell. a) 3rd vibrating mode with $\bar{t}$=0.25, Vf=54%, b) 9th vibrating mode with $\bar{t}$=0.75, Vf =41%. D=2 mm

3.3 Orthotropic Core

This subsection is focused on evaluating the effects of BBC cell's strut waviness on the modal behaviour. The geometry has been modified in order to design a BCC cell with curved struts with the following radii: R=10 mm, R=15 mm, R=20 mm. The corresponding BCC lattice cell with curved struts is presented in Figure 6. The properties of this cell's type have been then homogenised and inserted into the sandwich core. As in the previous subsection, various strut diameters have been considered, namely D=1 mm and D=2 mm. The sandwich plate has also a simply supported boundary condition along the lateral four sides. In Table 6 the frequencies for this structural case are shown, while in Figure 7 and Figure 8, some examples of the obtained vibrating modes are reported.

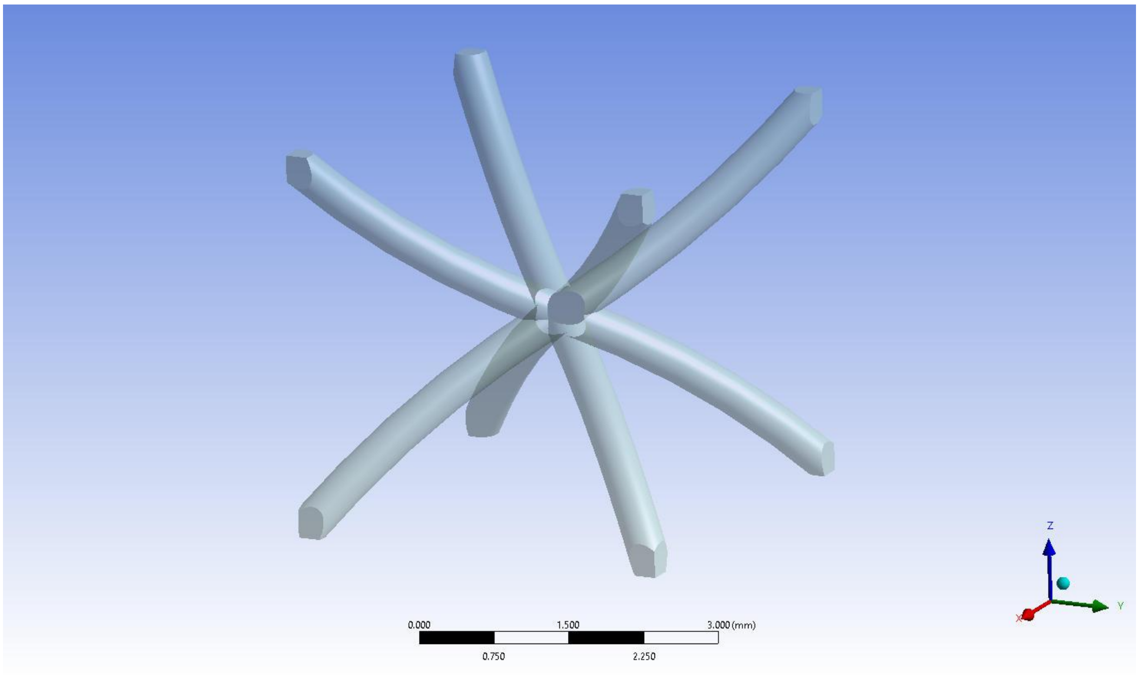

Fig. 6. Representation of the BCC lattice cell with curved struts, R=10 mm

Table 6
Natural frequencies of the curved strut case in Hz, in respect of the radii and diameters of the struts

Mode		1	2	3	4	5	6	7	8	9	10
	R=10	58.11	138.47	161.66	229.43	274.69	335.76	354.53	395.16	460.09	505.73
D=1	R=15	59.36	142.12	165.45	235.66	283.97	344.99	366.68	407.11	480.14	524
	R=20	60.1	143.91	167.49	238.59	287.56	349.22	371.28	412.14	486.21	530.51
	R=10	45.98	105.49	126.04	183.51	205.42	259.88	281.53	315.94	345.3	411.61
D=2	R=15	45.92	106.43	125.48	183.32	208.43	258.82	282.91	314.87	351.4	411.49
	R=20	46.24	107.64	126.31	184.63	211.33	260.65	285.59	316.94	356.75	414.53

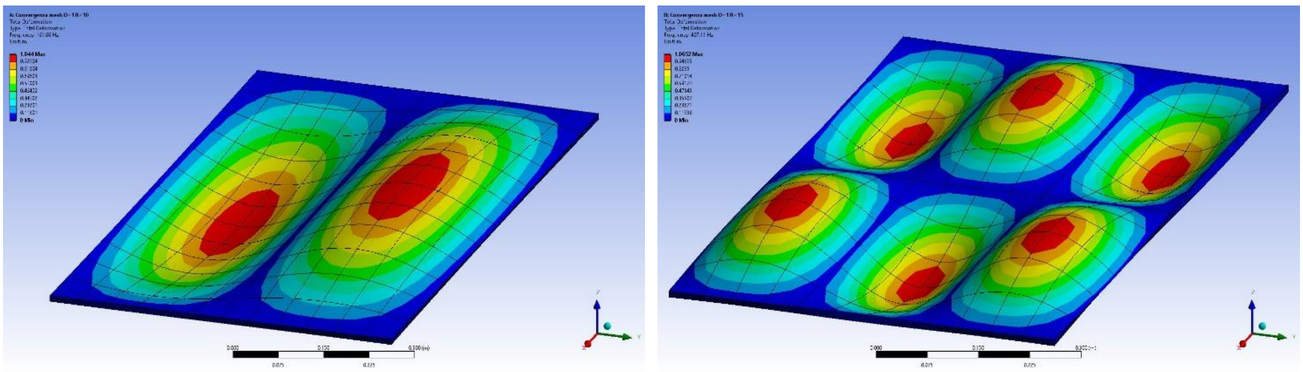

(a) (b)

Fig. 7. Sandwich plate with lattice cell. (a) 3rd vibrating mode for R=10, D=1 mm, (b) 8th vibrating mode for R=15 mm, D=1 mm

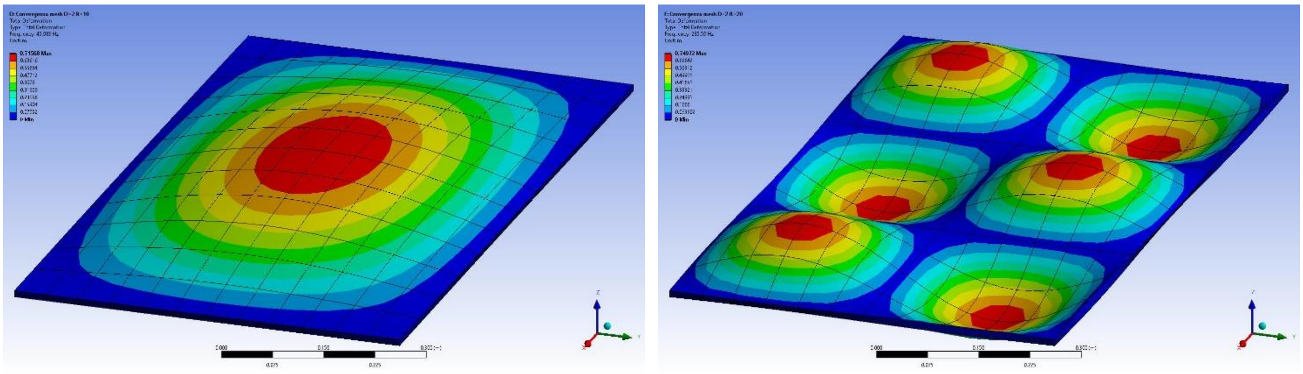

(a) (b)

Fig. 8. Sandwich plate with lattice cell. (a) 1st vibrating mode for R=10, D=2 mm, (b) 7th vibrating mode for R=20 mm, D=2 mm

4. Static Analysis

In this section, a static analysis is performed on the same sandwich structure investigated previously. The sandwich panel has been analysed using a multi scale approach, hence performing a static analysis of the whole homogenised panel first, and then considering the mesoscale zone with major deflections that is situated at the centre of the plate. The homogenised sandwich panel and the considered mesoscale zone for the multiscale analysis are depicted in Figure 9. A pressure load of 534 Pa is imposed on the top skin of sandwich structure, while a simply supported boundary condition is imposed along the four lateral sides of the plate. Moreover, the measure of the central zone for the second step of the multiscale analysis is 8 cm x 4 cm, while the single BCC cell side has a length of 4 mm. The BCC cell materials have been taken from Valvano [20].

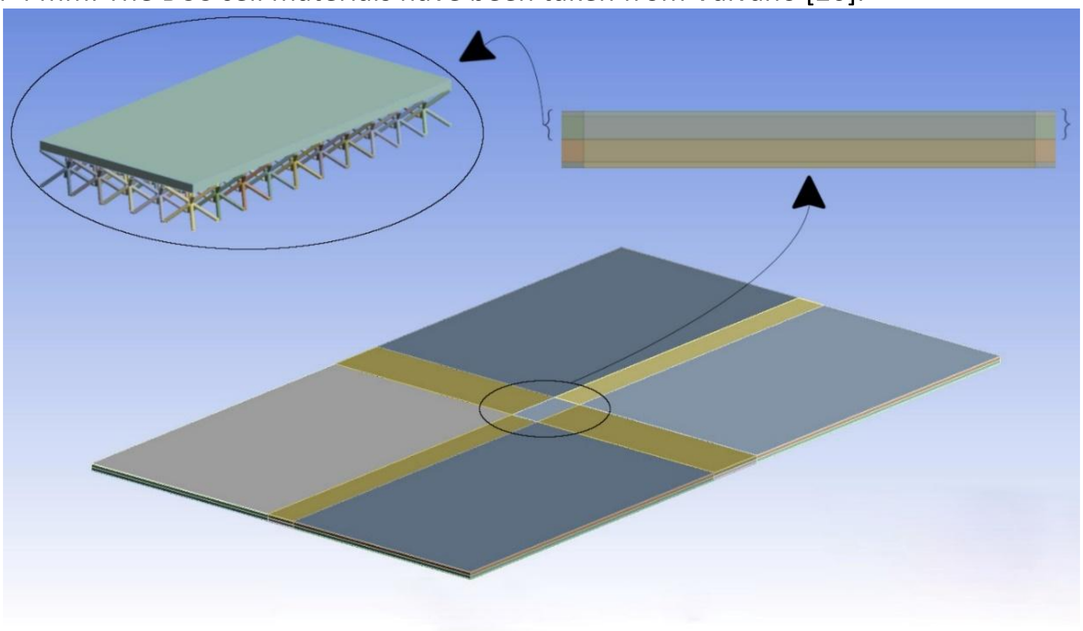

Fig. 9. Sandwich plate, highlight of the considered local zone for the multiscale analysis and placing of the BCC cells

4.1 Isotropic Core

In this section, a static analysis is performed on the sandwich panel, varying the strut's diameter of the straight BCC cell shown in Figure 1. In fact, two values have been chosen for the cell's diameter, namely: D=0.4 mm and D=0.8 mm, which correspond to an equivalent cell density of 388.69 kg/m^3 and 175.03 kg/m^3 respectively. As a consequence, the core of the considered portion of the sandwich panel is made up of 5x10 cells. For the mechanical evaluation, three outputs have been considered, namely: total deformation, Von Mises stress and maximum principal stress. Moreover, a path probe along the thickness of the structure has been defined for local evaluation of the considered variables. The path is defined along the top half of the plate thickness, as depicted in Figure 10 (a).

The total deformation of the local zone is shown in Figure 10 (b) with the highest deformation located in the centre plate. Similar global behaviour is obtained for the other considered strut diameter case. Figure 11 presents the Von Mises stresses for both the considered diameters of real sandwich panels. A stress concentration may be noticed on the junction between the top plate and the cells in both cases. Table 7 presents the quantitative data values of: the directional displacement w in the Z direction, normal σ_{xx} and σ_{zz} stresses. These values have been probed at the centre of the top skin, selecting the central node of the mesh, which coordinates are: x=0.5 m, y=0.3 m, z=0.01 m. An increase in the cell's diameter causes a decrease of the directional displacement w ($\sim 24.7\%$)and σ_{xx} stress ($\sim 25.7\%$), while σ_{zz} does not exhibit a significant variation. The comparison of the homogenised and real models shows perfect agreement for the deformation value. Whilst, taking into account the stresses, the maximum deviation between the real and the homogenised structures happens to be less than 2% for the D=0.4 mm case, and less than 10% for the D=0.8 mm case. The trend of the transverse displacement w is displayed in Figure 12 for both the considered diameters of homogenised and real sandwich structures. The trend of the homogenised structure follows quite well the one of the real structures. Furthermore, the same trends are reported for the principal stresses in Figure 13. In this case, the stresses' trends present some deviation from the real model; however, they appear to effectively represent the behaviour of the real structure near the skin zone. However, despite some localised effects, the model has proven to be representative of the global results, contributing to a decrease in the computational cost of the analysis. In fact, the Degrees Of Freedom (DOF) of the problem have decreased by two order of magnitude from the real structure to the homogenised case, passing from approximately 4500000 to 58368.

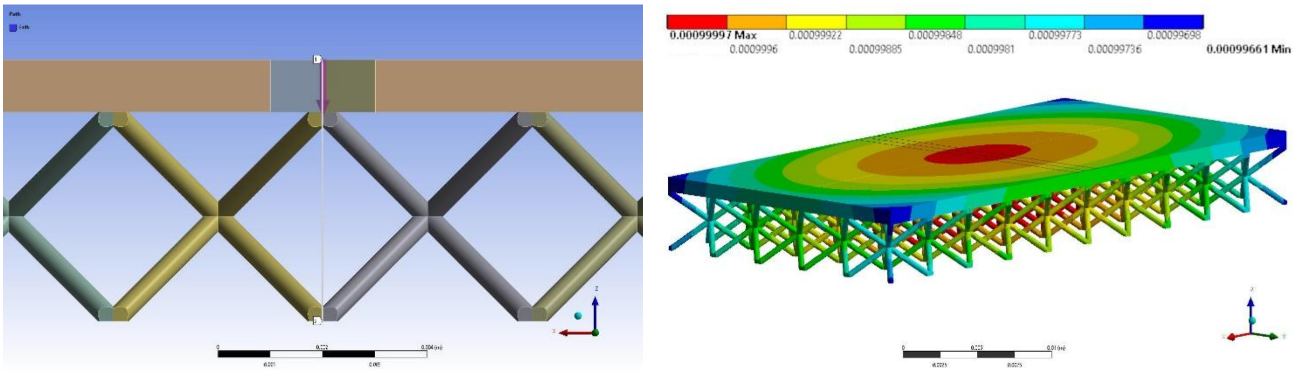

(a) (b)

Fig. 10. Sandwich plate with lattice core. (a) positioning of the measuring probe path, (b) total deformation for the D=0.4 mm case

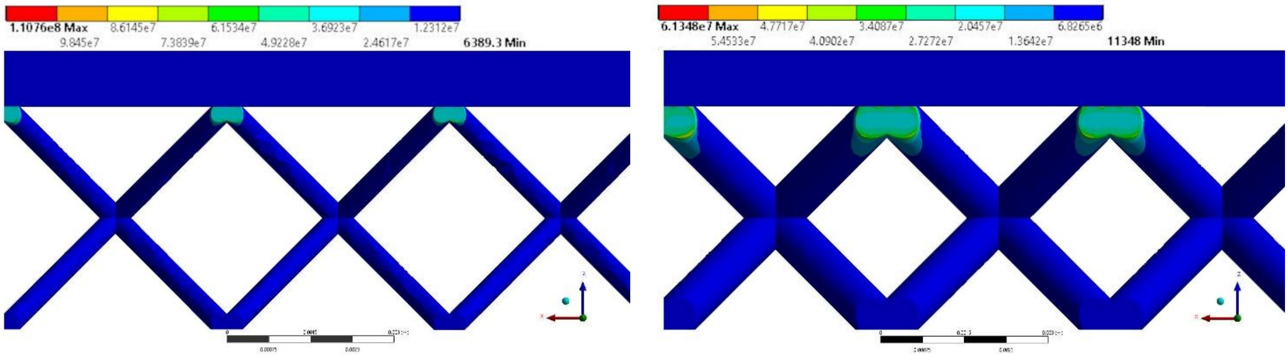

(a) (b)

Fig. 11. Sandwich plate, visualisation of the full considered local zone for the multiscale analysis. Von Mises stress for (a) D=0.4 mm and (b) D=0.8 mm

Table 7
Sandwich plate with lattice core, transverse displacement w and principal stresses evaluated at (x,y,z)=(a/2,b/2,+h/2) for the D=0.4 mm and D=0.8 mm case

	D=0.4 mm			D=0.8 mm		
	w [m]	σ_{xx} [Pa]	σ_{zz} [Pa]	w [m]	σ_{xx} [Pa]	σ_{zz} [Pa]
Homogenised	-9.997E-04	-2.597E+06	-5.349E+02	-7.529E-04	-1.929E+06	-5.347E+02
Real	-9.997E-04	-2.588E+06	-5.410E+02	-7.529E-04	-1.886E+06	-5.768E+02

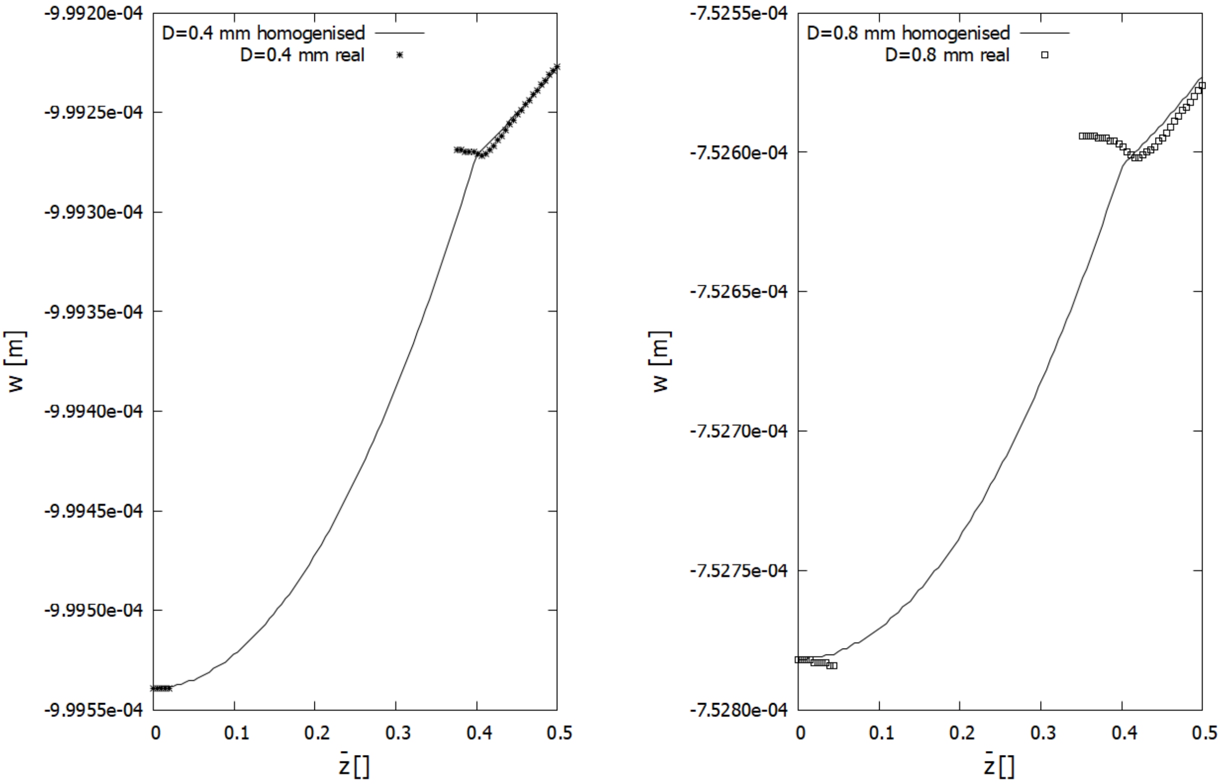

(a) (b)

Fig. 12. Sandwich plate with composite core, transverse displacement w evaluated at (x,y)=(0.5a,0.5b), for (a) D=0.4 mm and (b) D=0.8 mm

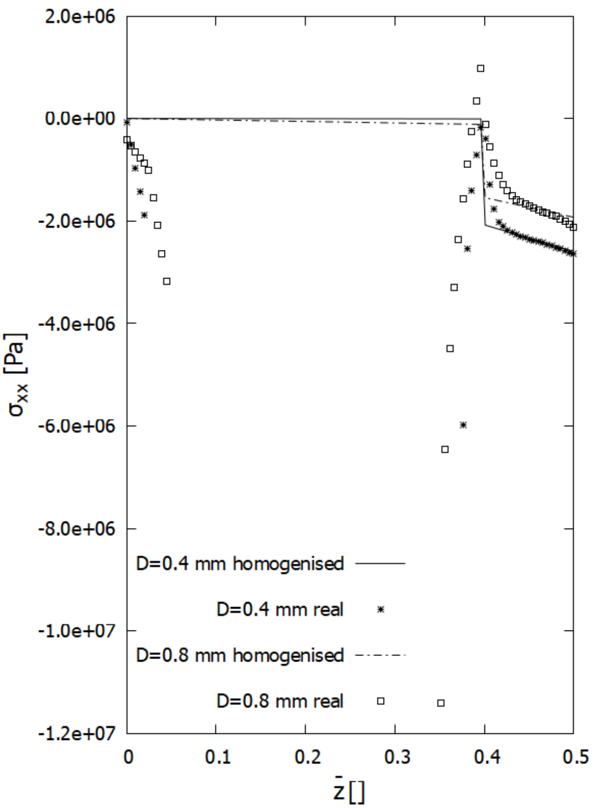

(a)

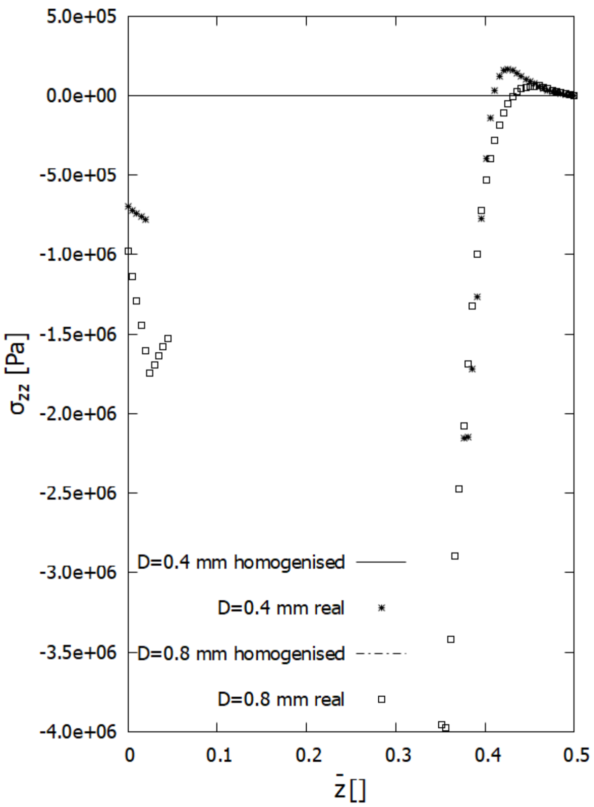

(b)

Fig. 13. Sandwich plate with composite core, normal stress along the (a) X axis and (b) Z axis evaluated at (x,y)=(0.5a,0.5b), for all the considered diameters

4.2 Composite Core

This section focuses on the effects of on the BCC cell's materials on the static analysis of the sandwich panel. The cell's geometry is the same as presented in Figure 3, with the layered strut configuration. For the present case, a volume fraction V_f=54% of the metal matrix composite AlSiC and a diameter D=0.8 mm have been chosen, while the strut's thickness ratio has been varied, focusing on three configurations, as follows: $\bar{t} = 0.25$, $\bar{t} = 0.50$ and $\bar{t} = 0.75$.

The deformation distribution of the considered structure remains the same with respect to the previous cases (Figure 10), hence this distribution is not reported for the sake of simplicity. The resulting Von Mises stress are depicted in Figure 14 for the $\bar{t} = 0.25$ and $\bar{t} = 0.75$ thickness ratios. In Table 8, the quantitative values of the aforementioned magnitudes are presented. In this case, the punctual values of the deformation vary from each other by 0.02% at most, while the stresses appear to deviate from the real structure, even if the maximum difference is less than 17%, specifically for the $\bar{t}$=0.5 case. In Figure 15, the trends of the transverse displacement w are presented for both cases. As for the previous section, the relative trends of the real and homogenised cases are highly comparable, apart from a negligible deviation.

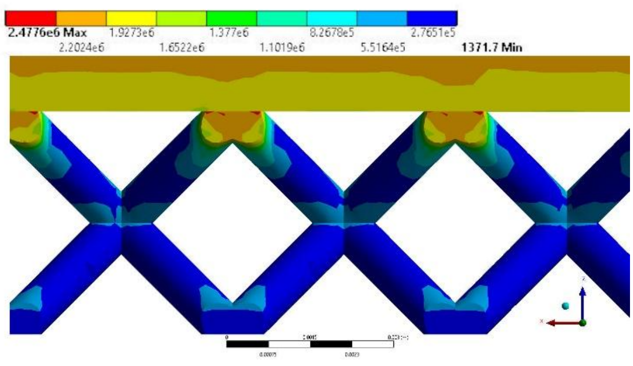

(a) (b)

Fig. 14. Sandwich plate, visualisation of the full considered local zone for the multiscale analysis. Von Mises stress for (a) $\bar{t}$ =0.25 and (b) $\bar{t}$ =0.75

Table 8
Sandwich plate with lattice core, transverse displacement w and principal stresses evaluated at (x,y,z)=(a/2,b/2,+h/2) stresses for the $\bar{t}$=0.25, $\bar{t}$=0.5, $\bar{t}$=0.75 case

	$\bar{t}$=0.25			$\bar{t}$=0.50			$\bar{t}$=0.75		
	w [m]	σ_{xx} [Pa]	σ_{zz} [Pa]	w [m]	σ_{xx} [Pa]	σ_{zz} [Pa]	w [m]	σ_{xx} [Pa]	σ_{zz} [Pa]
Hom.	-9.160E-04	-2.371E+06	-6.797E+02	-8.861E-04	-2.290E+06	-6.816E+02	-8.388E-04	-2.161E+06	-6.697E+02
Real	-9.158E-04	-2.346E+06	-5.691E+02	-8.860E-04	-2.266E+06	-5.657E+02	-8.387E-04	-2.139E+06	-5.643E+02

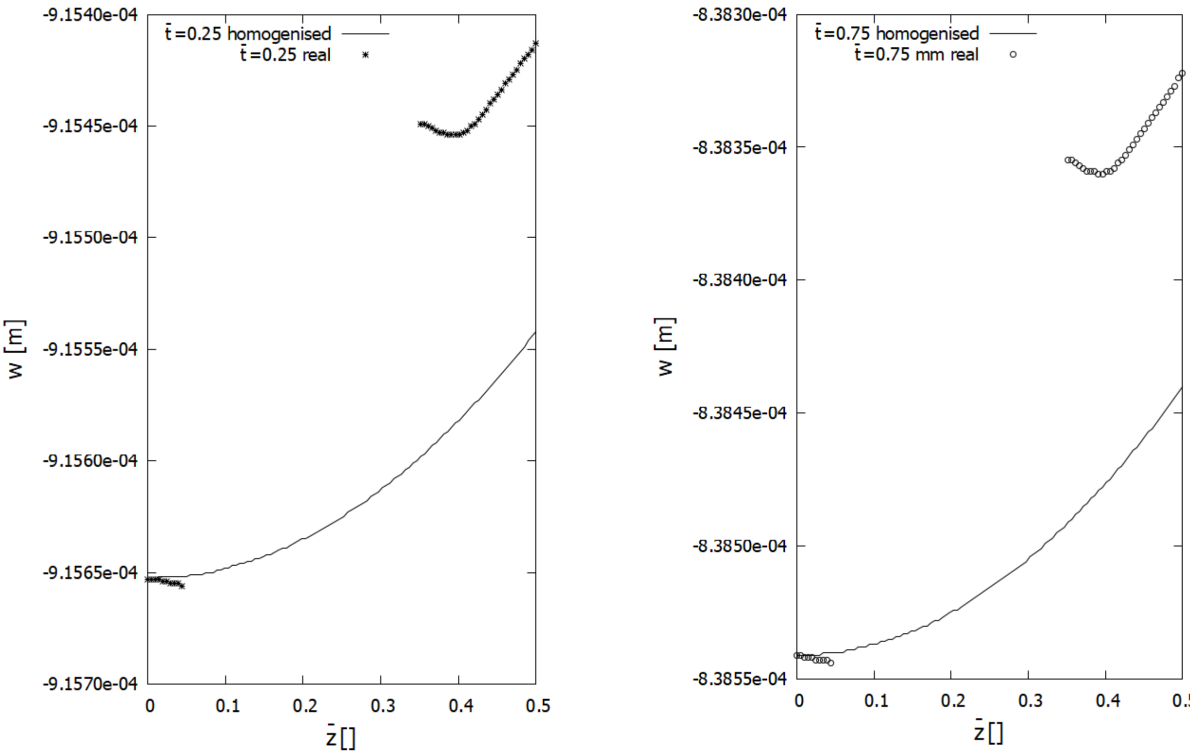

(a) (b)

Fig. 15. Sandwich plate with composite core, transverse displacement w evaluated at (x,y)=(0.5a,0.5b), for (a) $\bar{t}$=0.25 and (b) $\bar{t}$=0.75

Moreover, in Figure 16 the corresponding trends for the principal stresses are shown. Referring to the figure, it is clear how the normal stress σ_{xx} is better represented than σ_{zz}, as for the straight struts case. Regarding the total deformation, it can be noticed that it decreases as the thickness ratio increases, which is due to the increase of the AlSiC concentration in the cell's layered strut. Regarding the stresses instead, a noticeable difference in the stress concentration is present. In fact, further stress concentrations appear around the cell's centroid as the thickness ratio increases. Moreover, the implementation of layered struts causes a much more complicated stress distribution, as can be noticed by comparing Figure 14 and Figure 11 above. Specifically, apart from the cell-skin interface and the cell's centroid, even the skin seems to be affected by the introduction of the layered struts. The same trend and stress concentration are visible for the maximum principal stress. Furthermore, the implementation of a homogenised approach leads to a considerable reduction of the required computing resources. In fact, by comparing the DOF for the real and homogenised case, it must be noticed that those are again two orders of magnitude lower than the real case, thus maintaining an acceptable accuracy for the global effects evaluation. The DOF decreased from approximately 2500000 to 58368.

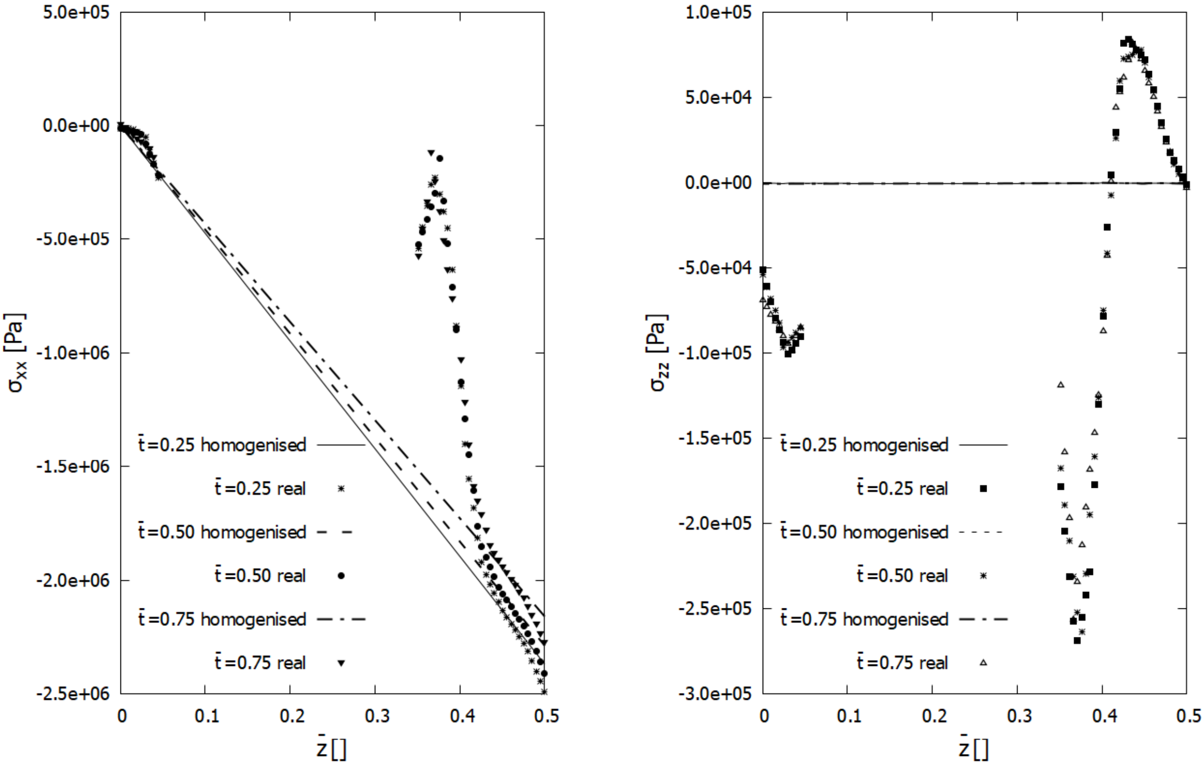

(a) (b)

Fig. 16. Sandwich plate with composite core, normal stress along the (a) X axis and (b) Z axis evaluated at (x,y)=(0.5a,0.5b), for all the considered thickness ratios

4.3 Orthotropic Core

In this last section, the focus was brought to the behaviour of the sandwich structure made of BCC lattice cells with curved struts. The cell's design is the same as presented in Figure 6. Three curvature radii have been chosen, namely R=10 mm, R=15 mm and R=20 mm, while the diameter has been fixed to D=0.4 mm.

Regarding the deformation distribution of the local zone, it must be noticed that it remains the same regardless of the waviness configuration, hence a single case is hereby reported, that is R=10 mm in Figure 17 (a).

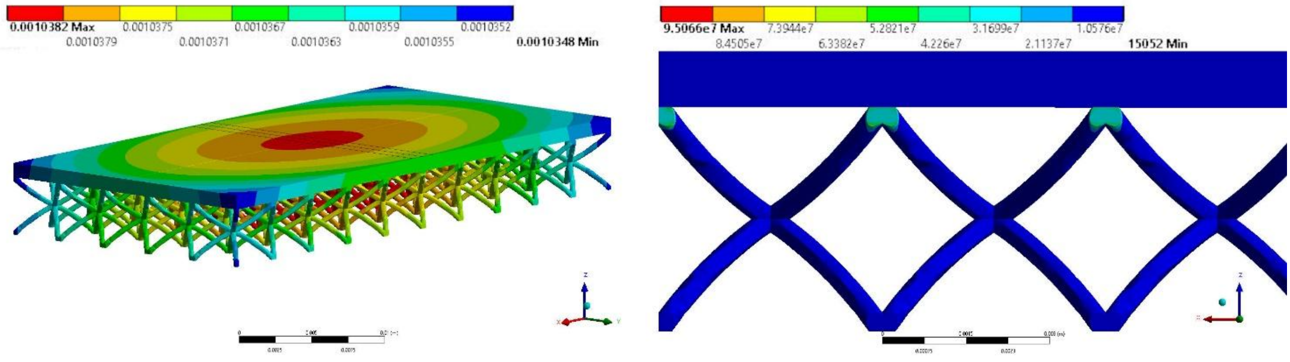

(a) (b)

Fig. 17. Sandwich plate, visualisation of the full considered local zone for the multiscale analysis for the R=10 mm radius configuration. (a) total deformation, (b) Von Mises stress

Table 9
Sandwich plate with lattice core, transverse displacement w and principal stresses evaluated at (x,y,z)=(a/2,b/2,+h/2) stresses for the R=10 mm, R=15 mm and R=20 mm case

	R=10 mm			R=15 mm			R=20 mm		
	w [m]	σ_{xx} [Pa]	σ_{zz} [Pa]	w [m]	σ_{xx} [Pa]	σ_{zz} [Pa]	w [m]	σ_{xx} [Pa]	σ_{zz} [Pa]
Hom.	-1.038E-03	-2.681E+06	-5.319E+02	-1.038E-03	-2.690E+06	-5.372E+02	-1.037E-03	-2.690E+06	-5.379E+02
Real	-1.038E-03	-2.679E+06	-5.336E+02	-1.038E-03	-2.686E+06	-5.300E+02	-1.037E-03	-2.684E+06	-5.427E+02

Moreover, the Von Mises stress is shown in Figure 17 (b) for the same radius configuration, the stress distribution appears to be similar to the straight struts case. Table 9 highlights the effects of the radius on the deformation and stresses. The introduction of the waviness didn't cause a further deviation from the real and the homogenised structures' behaviour. In fact, regarding the deformation, the difference between the two cases is null. Focusing on the stresses, the deviation is less than 1.5% at most. The displacement's trend is shown in Figure 18 for the waved struts configuration and is comparable for the homogenised and real structures. Regarding the two principal stresses those are presented in Figure 19. It must be noted that this time a better representation is provided in the σ_{xx} trend, as the homogenised model follows the real structure's behaviour accurately. The normal σ_{zz} stress presents a slight initial deviation from the expected trend, whereas the solution seems to converge at the value of the real structure near the skin region. As for the previous cases, the homogenised approach leads to a reduction of the computing cost, as it can be seen by comparing the DOF of the real case, which are approximately 3600000, to 58368 of the homogenised case.

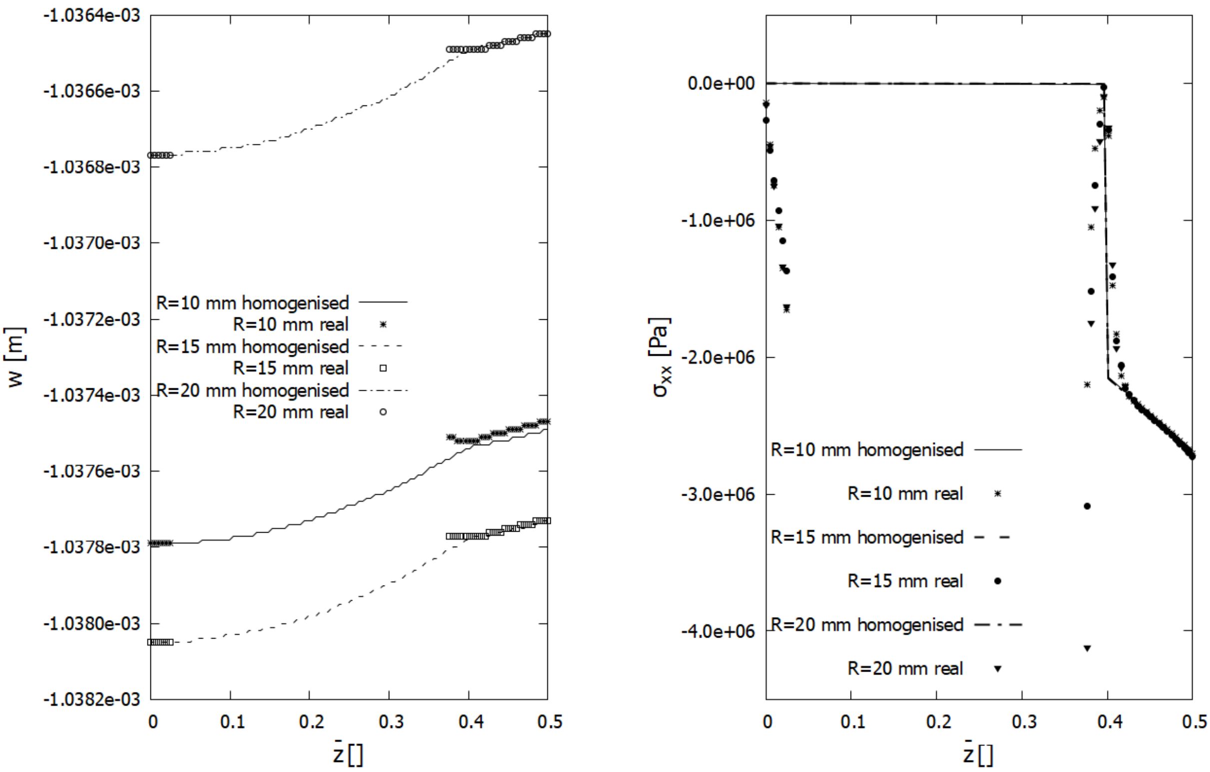

(a) (b)

Fig. 18. Sandwich plate with composite core, (a) transverse displacement w and (b) normal stress along the X axis evaluated at (x,y)=(0.5a,0.5b), for all the considered radii

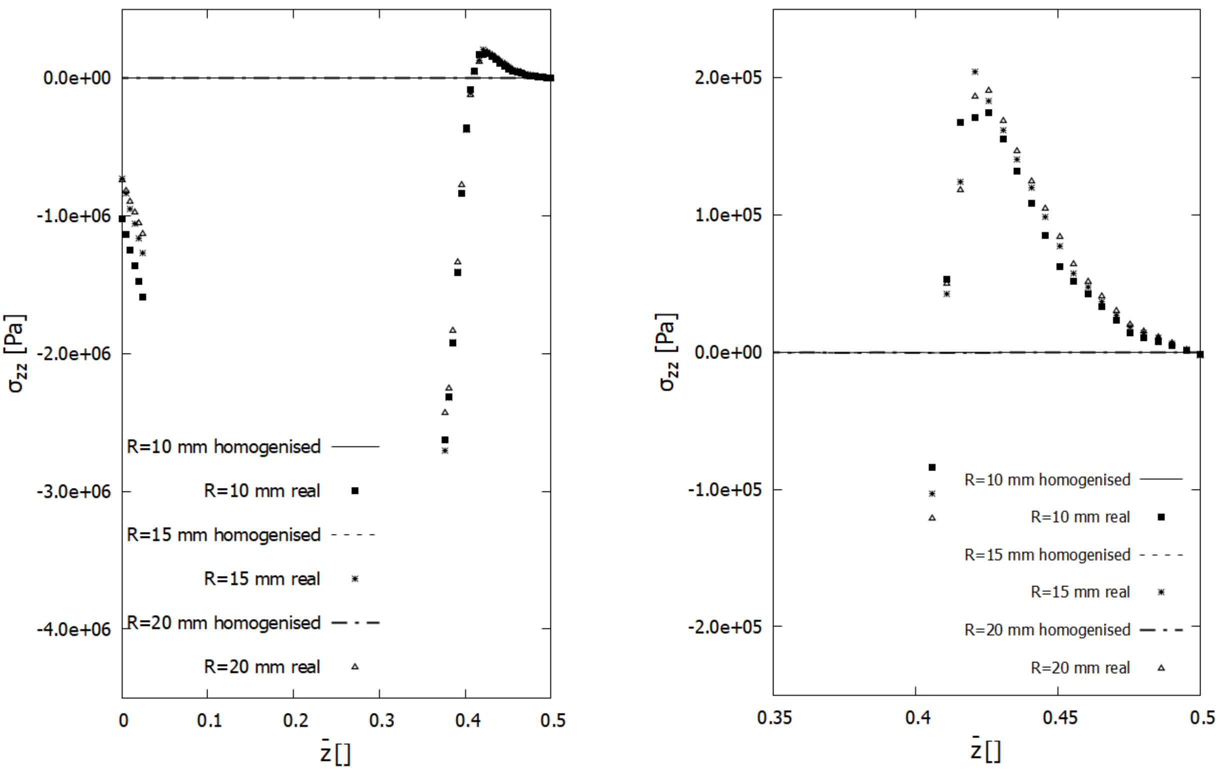

(a) (b)

Fig. 19. Sandwich plate with composite core, (a) normal stress along the Z axis evaluated at (x,y)=(0.5a,0.5b) and (b) highlight of the trend of the homogenised structures, for all the considered radii

5. Conclusions

In this work, a parametric study has been conducted on the modal and static response of sandwich panels with a lattice-structured core. The behaviour of the real structure has been compared with a homogenised model of the sandwich panel. A FEM approach with 3D quadratic elements has been implemented and a reduced integration has been set in order to enhance the accuracy of the model. The implemented geometry consists of elementary body centred cubic cells which constitute the core of the sandwich structure. Different designs of the BCC cell's struts have been made, in particular, three configurations have been studied. The first one consists of BCC cells with straight aluminium struts, while the other two involved BCC cells with composite layered struts and BCC cells with aluminium waved struts. The composite BCC cell's struts have been designed with an aluminium matrix and an AlSiC filler. The parametrisation of the study regarded the strut's diameter, waviness and thickness ratio of the respective BCC cells. The static analysis was conducted by the use of a multiscale approach, where the homogenised panel had been modelled first, then the same analysis was repeated for a small portion of the panel, and finally comparing the results of the homogenised structure with the real one. The results obtained from the analyses suggest the following conclusions:

i. The modal shapes of the sandwich panel and their corresponding frequencies do not exhibit noticeable differences with respect to the variation of the parameters of the three BCC cell configurations.
ii. The distribution of the total deformation remains constant with respect to the changes in diameter, waviness and thickness ratio.
iii. A stress concentration is present at the interface between the skin and the core, for both the BCC cell with straight and curved struts, contrary to the BCC cell with composite struts, where a much complicated stress distribution is detected.
iv. A tangible decrease of the transverse displacement is noticeable when the diameter and the thickness ratio are increased for the BCC cell with straight struts and composite struts respectively. The same behaviour is not visible for the waved struts BCC cells.
v. The trends of the real and homogenised structures are accurately represented for the transverse displacement w and the normal σ_{xx} stress, while the homogenised model presents some deviation from the real model for the normal σ_{zz} stress. However, the model's precision is sufficiently accurate near the skin region for all of the described magnitudes.
vi. Despite some deviations of the homogenised structure from the real one, the general trends of the transverse displacement and principal stresses are accurately represented.

Author Contributions

Conceptualization, M.P. and S.V.; methodology, S.V.; validation, F.M.; formal analysis, F.M.; investigation, F.M.; data curation, F.M., M.P. and S.V.; writing—original draft preparation, F.M.; writing—review and editing, F.M., M.P. and S.V.; supervision, M.P. and S.V.; All authors have read and agreed to the published version of the manuscript.

Funding

This research received no external funding.

Data Availability Statement

The data that support the findings of this study are available on request from the corresponding author.

Conflicts of Interest

The authors declare that they have no known competing financial interests or personal relationships that could have appeared to influence the work reported in this paper.

Acknowledgement

Federico Marino is supported by PhD funding from the College of Science and Engineering at the University of Derby.

References

[1] Rama, G., Marinkovic, D., & Zehn, M. (2018). High Performance 3-Node Shell Element for Linear and Geometrically Nonlinear Analysis of Composite Laminates. Composites Part B: Engineering, 151, 118-126. https://doi.org/10.1016/j.compositesb.2018.06.007

[2] Pei, E., & Kabir, I. (2022). Standardisation in AM. In: Godec, D., Gonzalez-Gutierrez, J., Nordin, A., Pei, E., Ureña Alcázar, J. (eds) A Guide to Additive Manufacturing. Springer Tracts in Additive Manufacturing. Springer, Cham. (pp. 59–73). https://doi.org/10.1007/978-3-031-05863-9_3

[3] Zhu, J., Zhou, H., Wang, C., Zhou, L., Yuan, S., & Zhang, W. (2021). A Review of Topology Optimization for Additive Manufacturing: Status and Challenges. Chinese Journal of Aeronautics, 34(1), 91-110. https://doi.org/10.1016/j.cja.2020.09.020

[4] Liu, J., Gaynor, A. T., Chen, S., Kang, Z., Suresh, K., Takezawa, A., Li, L., Kato, J., Tang, J., Wang, C. C. L., Cheng, L., Liang, X., & To, A. C. (2018). Current and Future Trends in Topology Optimization for Additive Manufacturing. Structural and Multidisciplinary Optimization, 57(6), 2457-2483. https://doi.org/10.1007/s00158-018-1994-3

[5] Berrocal, L., Fernández, R., González, S., Periñán, A., Tudela, S., Vilanova, J., Rubio, L., Martín Márquez, J. M., Guerrero, J., & Lasagni, F. (2019). Topology Optimization and Additive Manufacturing for Aerospace Components. Progress in Additive Manufacturing, 4, 83-95. https://doi.org/10.1007/s40964-018-0061-3

[6] Blakey-Milner, B., Gradl, P., Snedden, G., Brooks, M., Pitot, J., Lopez, E., Leary, M., Berto, F., & du Plessis, A. (2021). Metal Additive Manufacturing in Aerospace: A Review. Materials and Design, 209, 110008. https://doi.org/10.1016/j.matdes.2021.110008

[7] Leal, R., Barreiros, F. M., Alves, L., Romeiro, F., Vasco, J. C., Santos, M., & Marto, C. (2017). Additive Manufacturing Tooling for the Automotive Industry. International Journal of Advanced Manufacturing Technology, 92, 1671-1676. https://doi.org/10.1007/s00170-017-0239-8

[8] Sheoran, A. J., Kumar, H., Arora, P. K., & Moona, G. (2020). Bio-Medical Applications of Additive Manufacturing: A Review. Procedia Manufacturing, 51, 663-670. https://doi.org/10.1016/j.promfg.2020.10.093

[9] Dörfler, K., Dielemans, G., Lachmayer, L., Recker, T., Raatz, A., Lowke, D., & Gerke, M. (2022). Additive Manufacturing Using Mobile Robots: Opportunities and Challenges for Building Construction. Cement and Concrete Research, 158, 106772. https://doi.org/10.1016/j.cemconres.2022.106772

[10] Gibson, L. J. (2003). Cellular Solids. MRS Bulletin, 28(4), 270-274. https://doi.org/10.1557/mrs2003.79

[11] Ashby, M. F. (2006). The Properties of Foams and Lattices. Philosophical Transactions of the Royal Society A: Mathematical, Physical and Engineering Sciences, 364(1838), 15-30. https://doi.org/10.1098/rsta.2005.1678

[12] Fleck, N. A (2004). An Overview of the Mechanical Properties of Foams and Periodic Lattice Materials. Cellular Metals and Polymers, 3-7.

[13] Evans, A. G., Hutchinson, J. W., Fleck, N. A., Ashby, M. F., & Wadley, H. N. G. (2001). The Topological Design of Multifunctional Cellular Metals. Progress in Materials Science, 46(3-4), 309-327. https://doi.org/10.1016/S0079-6425(00)00016-5

[14] Fleck, N. A., Deshpande, V. S., & Ashby, M. F. (2010). Micro-Architectured Materials: Past, Present and Future. Proceedings of the Royal Society A: Mathematical, Physical and Engineering Sciences, 466(2121), 2495-2516. https://doi.org/10.1098/rspa.2010.0215

[15] Bai, L., Yi, C., Chen, X., Sun, Y., & Zhang, J. (2019). Effective Design of the Graded Strut of BCC Lattice Structure for Improving Mechanical Properties. Materials, 12(13), 2192. https://doi.org/10.3390/ma12132192

[16] Alaña, M., Lopez-Arancibia, A., Pradera-Mallabiabarrena, A., & Ruiz de Galarreta, S. (2019). Analytical Model of the Elastic Behavior of a Modified Face-Centered Cubic Lattice Structure. Journal of the Mechanical Behavior of Biomedical Materials, 98, 357-368. https://doi.org/10.1016/j.jmbbm.2019.05.043
[17] Qi, D., Yu, H., Liu, M., Huang, H., Xu, S., Xia, Y., Qian, G., & Wu, W. (2019). Mechanical Behaviors of SLM Additive Manufactured Octet-Truss and Truncated-Octahedron Lattice Structures with Uniform and Taper Beams. International Journal of Mechanical Sciences, 163, 105091. https://doi.org/10.1016/j.ijmecsci.2019.105091
[18] Pan, C., Han, Y., & Lu, J. (2020). Design and Optimization of Lattice Structures: A Review. Applied Sciences, 10(18), 6374. https://doi.org/10.3390/APP10186374
[19] Tumino, D., Alaimo, A., Mantegna, G., Orlando, C., & Valvano, S. (2023). Mechanical Properties of BCC Lattice Cells with Waved Struts. International Journal on Interactive Design and Manufacturing, 1-14. https://doi.org/10.1007/s12008-023-01359-9
[20] Valvano, S. (2024). Homogenised Properties of Lattice Metal Composite Cell. Facta Universitatis, Series: Mechanical Engineering. https://doi.org/10.22190/FUME240125015V
[21] Lu, H., Deng, W., Luo, K., Chen, Y., Wang, J., & Lu, J. (2023). Tailoring Microstructure of Additively Manufactured Ti6Al4V Titanium Alloy Using Hybrid Additive Manufacturing Technology. Additive Manufacturing, 63, 103416. https://doi.org/10.1016/j.addma.2023.103416
[22] An, L., Guo, Z., Li, Z., Fu, Y., Hu, Y., Huang, Y., Yao, F., Zhou, C., & Ren, S. (2022). Tailoring Thermal Insulation Architectures from Additive Manufacturing. Nature Communications, 13(1), 4309. https://doi.org/10.1038/s41467-022-32027-3
[23] Chen, N., He, C., & Pang, S. (2022). Additive Manufacturing of Energetic Materials: Tailoring Energetic Performance via Printing. Journal of Materials Science and Technology, 127, 29-47. https://doi.org/10.1016/j.jmst.2022.02.047
[24] Pollock, T. M., Clarke, A. J., & Babu, S. S. (2020). Design and Tailoring of Alloys for Additive Manufacturing. Metallurgical and Materials Transactions A: Physical Metallurgy and Materials Science, 51, 6000-6019. https://doi.org/10.1007/s11661-020-06009-3
[25] Plocher, J., & Panesar, A. (2019). Review on Design and Structural Optimisation in Additive Manufacturing: Towards next-Generation Lightweight Structures. Materials and Design, 183, 108164. https://doi.org/10.1016/j.matdes.2019.108164
[26] Hill, R. (1963). Elastic Properties of Reinforced Solids: Some Theoretical Principles. Journal of the Mechanics and Physics of Solids, 11(5), 357-372. https://doi.org/10.1016/0022-5096(63)90036-X
[27] Gitman, I. M., Askes, H., & Sluys, L. J. (2007). Representative Volume: Existence and Size Determination. Engineering Fracture Mechanics, 74(16), 2518-2534. https://doi.org/10.1016/j.engfracmech.2006.12.021
[28] Borbély, A., Biermann, H., & Hartmann, O. (2001). FE Investigation of the Effect of Particle Distribution on the Uniaxial Stress-Strain Behaviour of Particulate Reinforced Metal-Matrix Composites. Materials Science and Engineering: A, 313(1-2), 34-45. https://doi.org/10.1016/S0921-5093(01)01144-3
[29] Savvas, D., Stefanou, G., & Papadrakakis, M. (2016). Determination of RVE Size for Random Composites with Local Volume Fraction Variation. Computer Methods in Applied Mechanics and Engineering, 305, 340-358. https://doi.org/10.1016/j.cma.2016.03.002
[30] Omairey, S. L., Dunning, P. D., & Sriramula, S. (2019). Development of an ABAQUS Plugin Tool for Periodic RVE Homogenisation. Engineering with Computers, 35, 567-577. https://doi.org/10.1007/s00366-018-0616-4
[31] Ptochos, E., & Labeas, G. (2012). Elastic Modulus and Poisson's Ratio Determination of Micro-Lattice Cellular Structures by Analytical, Numerical and Homogenisation Methods. Journal of Sandwich Structures and Materials, 14(5), 597-626. https://doi.org/10.1177/1099636212444285
[32] Arabnejad, S., & Pasini, D. (2013). Mechanical Properties of Lattice Materials via Asymptotic Homogenization and Comparison with Alternative Homogenization Methods. International Journal of Mechanical Sciences, 77, 249-262. https://doi.org/10.1016/j.ijmecsci.2013.10.003
[33] Craster, R. V., Kaplunov, J., & Postnova, J. (2010). High-Frequency Asymptotics, Homogenisation and Localisation for Lattices. Quarterly Journal of Mechanics and Applied Mathematics, 63(4), 497-519. https://doi.org/10.1093/qjmam/hbq015
[34] Alaimo, A., Marino, F., & Valvano, S. (2021). BCC Lattice Cell Structural Characterization. Reports in Mechanical Engineering, 2(1), 77-85. https://doi.org/10.31181/rme200102077v77
[35] Mantegna, G., Vindigni, C. R., Valvano, S., Esposito, A., Tumino, D., Alaimo, A., & Orlando, C. (2023). Representative Volume Element Homogenisation Approach to Characterise Additively Manufactured Porous Metals. Mechanics of Advanced Materials and Structures, 30(5), 1073-1082. https://doi.org/10.1080/15376494.2022.2124002
[36] Ha, G. X., Zehn, M. W., Marinkovic, D., & Fragassa, C. (2019). Dealing with Nap-Core Sandwich Composites: How to Predict the Effect of Symmetry. Materials, 12(6), 874. https://doi.org/10.3390/ma12060874

[37] Ha, G. X., Marinkovic, D., & Zehn, M. W. (2019). Parametric Investigations of Mechanical Properties of Nap-Core Sandwich Composites. Composites Part B: Engineering, 161, 427-438. https://doi.org/10.1016/j.compositesb.2018.12.108

[38] Carrera, E., Valvano, S., & Filippi, M. (2018). Classical, Higher-Order, Zig-Zag and Variable Kinematic Shell Elements for the Analysis of Composite Multilayered Structures. European Journal of Mechanics, A/Solids, 72, 97-110. https://doi.org/10.1016/j.euromechsol.2018.04.015

[39] Alaimo, A., Orlando, C., & Valvano, S. (2019). An Alternative Approach for Modal Analysis of Stiffened Thin-Walled Structures with Advanced Plate Elements. European Journal of Mechanics, A/Solids, 77, 103820. https://doi.org/10.1016/j.euromechsol.2019.103820

[40] Hughes, T. J. R., Cohen, M., & Haroun, M. (1978). Reduced and Selective Integration Techniques in the Finite Element Analysis of Plates. Nuclear Engineering and Design, 46(1), 203-222. https://doi.org/10.1016/0029-5493(78)90184-X